Formulation of a Wall Model for LES in a Collocated Finite-Volume Framework

Mattias Liefvendahl, Timofey Mukha, Saleh Rezaeiravesh

Department of Information Technology
Uppsala University
Box 337, SE-751 05 Uppsala, Sweden

Technical report 2017-001
January 2017
ISSN 1404-3203

Contents

1 Introduction

Large-eddy simulation (LES) of wall-bounded flows puts significantly more stringent requirements on the grid resolution and the subgrid stress (SGS) modelling, as compared to LES of turbulent flows away from walls. The main reason for this is the structure of turbulence in boundary layers, with the size of energetic eddies being on the viscous length scale, $\delta_\nu = \nu/u_\tau$, where ν is the kinematic viscosity, $u_\tau = \sqrt{\tau_w/\rho}$, with τ_w denoting the wall shear stress, and ρ the fluid density, [24, 5, 23]. These flow structures mainly occur in the inner part of the turbulent boundary layer (TBL), at wall-normal distances below $\approx 30\delta_\nu$. In the outer layer the local TBL thickness, δ, is the relevant length scale. It is typically much larger than δ_ν, and the quotient δ/δ_ν grows rapidly with the increase of the Reynolds (Re-)number.

Aiming to resolve the energetic structures in the flow, including in the inner part of the TBL, is referred to as wall-resolved LES (WRLES), [5, 23, 6]. This leads, however, to a very rapid increase in the computational cost with the Re-number, due to the above-mentioned increase in δ/δ_ν, and the related grid resolution requirements, see [5, 6, 22] for estimates of the number of grid points necessary. This motivates introducing special modelling for the inner part of the TBL, essentially aiming to resolve only the larger flow structures in the boundary layer, on the length scale δ (and not to resolve the much smaller length scale δ_ν). This general approach is referred to as wall-modelled LES (WMLES), see [23, 20, 13] for reviews of this concept.

The purpose of this report is to provide a detailed presentation of one widely used wall model. Following the classification and terminology of the recent review [13], the considered model belongs to the class of so-called wall-stress models. Such models attempt to provide the correct value of the wall shear stress without modifying the location of the boundary of the LES domain. Here the model is formulated for incompressible flow, and in a collocated finite-volume framework, allowing for unstructured grids and arbitrary polyhedral cells. This computational fluid dynamics approach is generally used in software designed for handling complex geometries and industrial applications. In particular, this wall model is available in `OpenFOAM`[1], [27, 15], an open source software package. The wall model is local, in the sense that it employs only information from one finite-volume cell, the one adjacent to the cell face at the wall for which the stress is to be computed. A key component in the wall model is to employ the expression for a "law of the wall" suggested by Spalding, [26], which is valid from the wall and throughout the viscous sublayer, the buffer layer, and the log-law region. Similar wall models were suggested in early papers, [25, 10], typically employing the log-law and being formulated on a structured computational grid with a staggered grid configuration. Essentially all the components of the wall model presented here have been discussed by de Villiers [7] and also Fureby [9]. However, this report is the first publication entirely focused on providing a complete description of this wall model. Additionally, some remarks concerning the model's derivation, use, and possible modifications are given.

The report is structured as follows. In Section 2, the necessary background information

[1] `www.openfoam.com`

concerning LES and the finite-volume framework is first introduced, and then the wall model is described in Section 3.2. The performance of the model is then illustrated by WMLES simulation results for channel flow, and a comparison with DNS results, [14], see Section 4. Concluding remarks are given in the final section.

2 CFD framework

The necessary prerequisite information concerning LES and the finite-volume method is presented in this section, and then the wall model is formulated in the next section.

2.1 Large-eddy simulation

The governing equations are obtained by applying a filter to the incompressible Navier-Stokes equations, see e.g. [23]. Assuming that the filter operation commutes with the derivatives, the conservation of momentum and the incompressibility constraint are obtained in the following form in a Cartesian coordinate system,

$$\begin{aligned} \frac{\partial \overline{v}_i}{\partial t} + \frac{\partial}{\partial x_j}(\overline{v}_i \overline{v}_j) &= -\frac{1}{\rho}\frac{\partial \overline{p}}{\partial x_i} + \frac{\partial \tau_{ij}}{\partial x_j}, \quad (i = 1, 2, 3) \\ \frac{\partial \overline{v}_j}{\partial x_j} &= 0. \end{aligned} \tag{1}$$

A repeated index in a term implies summation over that index, and a bar over the variables indicates that they are filtered. The components of velocity are denoted v_i (and hence the filtered components are denoted $\overline{v}_i$), the density is ρ, the pressure p and τ_{ij} denotes the total deviatoric stress tensor. The stress tensor consists of two terms, the resolved and subgrid contributions respectively,

$$\tau_{ij} = 2\nu \overline{s}_{ij} + \tau_{ij}^{\text{sgs}}, \tag{2}$$

where

$$\overline{s}_{ij} = \frac{1}{2}\left(\frac{\partial \overline{v}_i}{\partial x_j} + \frac{\partial \overline{v}_j}{\partial x_i}\right),$$

is the filtered strain rate tensor, ν is the kinematic viscosity of the fluid, and

$$\tau_{ij}^{\text{sgs}} = \overline{v}_i \overline{v}_j - \overline{v_i v_j}, \tag{3}$$

is the subgrid stress tensor. Deriving computable expressions for τ_{ij}^{sgs} constitutes the subject of subgrid stress modelling. The discussion of wall-stress models presented below can, however, be carried out independently of the subgrid stress modelling away from the walls. This will be made clear in Section 3.1 below, where it is shown how the wall stress appears as a term in the discretised form of the integral formulation of the momentum equation.

Apart from a suitable SGS model, the equations (1) have to be complemented with initial and boundary conditions. In the context of this report it suffices to discuss what

boundary conditions are prescribed at the walls. However, it is necessary to strictly define the filter used for obtaining (1) before the boundary conditions can be considered. This, in turn, has to be preceded by a discussion of the employed numerical method. Therefore boundary conditions are discussed in detail below, in Section 2.3.

2.2 Finite-volume formulation

The collocated finite-volume discretisation is outlined in this section for a generic scalar transport equation of the form,

$$\frac{\partial \alpha}{\partial t} + \frac{\partial}{\partial x_i}(\alpha v_i) = \frac{\partial}{\partial x_i}\left(\Gamma \frac{\partial \alpha}{\partial x_i}\right) + s\,. \tag{4}$$

Here α is the transported scalar, v_i are the components of the velocity field (which transports the scalar), Γ is a diffusion coefficient, and s is a source term.

Only the parts of the discretisation which are necessary for the treatment of the wall shear stress are discussed here. It is referred to [8], and the references therein, for a more complete description.

The starting point for the finite-volume formulation is the integral form of equation (4), which is obtained by integrating the equation over a control volume V, with bounding surface S, and applying Gauss' theorem to the convective and the diffusive terms. The result is the following, where n_i are the components of the outward-pointing unit vector normal to S,

$$\frac{\mathrm{d}}{\mathrm{d}t}\int_V \alpha \,\mathrm{d}V + \oint_S \alpha v_i n_i \,\mathrm{d}S = \oint_S \Gamma \frac{\partial \alpha}{\partial x_i} n_i \,\mathrm{d}S + \int_V s \,\mathrm{d}V. \tag{5}$$

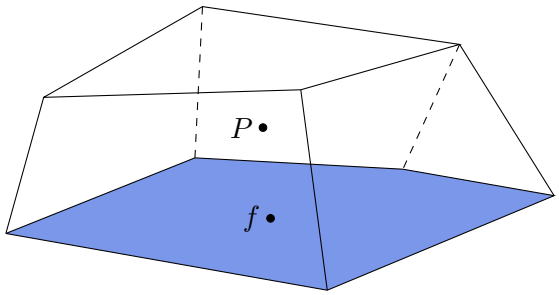

Figure 1: A finite-volume polyhedral cell. The cell-centre point is indicated by P, and the centre of the bottom (pentagonal) cell face is indicated by f.

The computational domain is divided into general polyhedral cells, or control volumes, see Figure 1 for an example, and then equation (5) is applied to each cell. The surface S of the cell V is then divided into a number, N_f, of polygonal faces S_f, so that,

$$S = \bigcup_{f=1}^{N_f} S_f.$$

The discretisation is then constructed aiming for second-order accuracy. In the collocated formulation, the unknown is taken at the cell centres, α_P. Notation is also introduced for the face flux, $\phi = v_i n_i$, and the gradient projected on the face normal,

$$\frac{\partial \alpha}{\partial n} = \frac{\partial \alpha}{\partial x_i} n_i.$$

Now all the necessary notation has been introduced for the formulation of the semi-discrete version of equation (5),

$$V \frac{\mathrm{d}\alpha_P}{\mathrm{d}t} + \sum_{f=1}^{N_f} \alpha_f \phi_f S_f = \sum_{f=1}^{N_f} \Gamma_f \left(\frac{\partial \alpha}{\partial n} \right)_f S_f + V s_P. \tag{6}$$

Here a subscript f implies evaluation in the face centre, and S_f is also used to denote the area of the corresponding face. In order to complete the spatial discretisation of the momentum equation, interpolation between the cell centres to obtain the face-centre values is required. Furthermore, time discretisation must be addressed.

These components of the algorithm are, however, not necessary for the purpose of the present report, and it is referred to e.g. [8] for more information.

2.3 Implicit filtering

No strict definition of the filter used to obtain the governing equations (1) has hitherto been given. The reason for this is that the filtering is in fact not performed explicitly. Instead, the filter kernel is defined as the reciprocal of the (local) volume of the cell. That is, filtering is being made equivalent to taking the average value of the unknown across V. Since in the collocated finite-volume method the cell average is represented by the value at the cell centre, the numerical method performs the filtering implicitly.

This approach is reasonable due to the fact that the cell size introduces a natural length scale which determines the size of the eddies that can be resolved. Also, removing the need for explicit filtering saves computational resources. What is important for further discussion is that the value of any flow quantity taken at the centre of a cell is equivalent to the filtered value of that quantity at the same location.

Having defined the filter it is now possible to resume the discussion of boundary conditions for the governing equations (1). For the non-filtered components of velocity the no-slip condition applies at the wall, whereas for the non-filtered pressure a homogeneous Neumann condition is appropriate. The question is, however, whether it is reasonable to assume that the same conditions are to be used for the filtered quantities. It can be shown that this is indeed the case only when the width of the filter used to obtain (1) decreases sufficiently when approaching the wall [23, 1]. For the type of filtering employed here this is equivalent to saying that the resolution of the computational grid next to the wall must be sufficiently fine.

The above condition is naturally satisfied in the case of WRLES, where the resolution of the inner layer sets stringent requirements on the mesh size. However, in WMLES the grid size does not decrease in the same manner, since the aim is only the resolution

of the outer layer of the TBL. In spite of this fact, the no-slip condition is still employed here for $\overline{v}_i$ along with the homogeneous Neumann condition for $\overline{p}$. These conditions are in fact also appropriate when used with WMLES, if the wall shear stress is treated in the way described in the next section.

3 Wall model formulation

First, it is explained how the wall shear stress is related to the LES-filtering and the finite-volume discretisation. Then the procedure for enforcing the wall shear stress, using Spalding's law of the wall, is described.

3.1 The wall shear stress

Consider a finite-volume cell with one face ($f = w$) being a part of a wall boundary. For simplicity, assume also that the wall lies in the x_1-x_3 plane. Then, for the tangential components, the integral form of the momentum equation (1) reads,

$$\frac{\mathrm{d}}{\mathrm{d}t}\int_V \overline{v}_i \,\mathrm{d}V + \oint_S \overline{v}_i\overline{v}_j n_j \mathrm{d}S = -\frac{1}{\rho}\oint_S \overline{p} n_i \,\mathrm{d}S + \oint_S \tau_{ij} n_j \,\mathrm{d}S. \qquad (i = 1, 3) \qquad (7)$$

Consider the last term in the above equation. As discussed in Section 2.1, it accounts for the effects of the subgrid scale and viscous fluxes. In the finite-volume framework the surface integral is decomposed into a sum over the faces of the considered cell, as was illustrated in Section 2.2. The contribution to the sum from the face at the wall is obtained as

$$\int_{S_w} \tau_{ij} n_j \mathrm{d}S = -\int_{S_w} \tau_{i2} \,\mathrm{d}S \approx \overline{\tau}_{w,i2} S_w. \qquad (i = 1, 3) \qquad (8)$$

Here the fact that the face normal points in the negative x_2 direction was used, $n_j = -\delta_{j2}$. The quantities $\overline{\tau}_{w,12}$ and $\overline{\tau}_{w,32}$ are the two non-zero components of the computed wall shear stress vector, which is parallel to the wall. The magnitude of this vector is referred to as $\overline{\tau}_w$. Note that the wall shear stress τ_w varies on a smaller scale ($\sim \delta_\nu$) than the cell face. The computed wall shear stress $\overline{\tau}_w$ should be interpreted as the average (or filtered) value over the boundary face.

3.2 Description of the wall model

The details of the wall model, and its relation to the discrete equations, are presented in the four following sub-sections.

3.2.1 Wall-stress models

In WMLES it is the job of the wall model to provide the wall stress's correct value. Different approaches to wall modelling have been developed [23, 13, 20]. Some involve solving a separate set of equations in the inner layer, thus shifting the domain of the

large-eddy simulation away from the wall. The model focused on in this report, however, falls under the class of so-called wall-stress models. Models of this type aim at directly enforcing the correct local value of the wall shear stress, with the domain of the LES simulation still extending all the way to the wall. The mode of operation of such models can be summarized in the following three steps.

Step 1 The values of $\overline{v}$, $\overline{p}$, or quantities derived from them (the pressure gradient, a certain component of $\overline{v}$, etc) are sampled from a point in the simulation domain, the location of which is somehow related to the location of f (the centre of the face on the wall, see Figure 1). The sampled values serve as input to the wall model.

Step 2 From the sampled input values, the local value of the wall shear stress $\overline{\tau}_w$ (or its components) is computed.

Step 3 The wall shear stress $\overline{\tau}_w$ computed by the model is in some way enforced at the given face centre. This is the way the model affects the solution to (1).

Within this common framework, the various models (and their implementations) differ in the concrete way these three steps are defined.

3.2.2 The Spalding law of the wall

When describing a wall model it is natural to start with Step 2 of the above algorithm. Among the different methods available for estimating the wall shear stress within the wall-stress models' framework, [23, 13], the considered model uses a wall function, an approach pioneered by Schumann [25] and further developed by Grötzbach [10].

The underlying idea is that the profile of the mean wall-parallel component of velocity in a TBL in equilibrium can be described by a functional relationship, a so-called law of the wall. This law can, in turn, be utilized to correlate the velocity at a specific point away from the wall to the local wall shear stress.

In the present study, the Spalding law of the wall [26] is employed. It describes the viscous sublayer, the buffer and logarithmic layers of a TBL's mean wall-parallel velocity profile through a single relation. Denoting the mean value (time or ensemble) with $\langle\cdot\rangle$, this law is written as,

$$\langle u\rangle^+ + e^{-\kappa B}\left[e^{\kappa\langle u\rangle^+} - 1 - \kappa\langle u\rangle^+ - \frac{1}{2}(\kappa\langle u\rangle^+)^2 - \frac{1}{6}(\kappa\langle u\rangle^+)^3\right] - y^+ = 0, \tag{9}$$

in which u is the wall-parallel component of velocity, y is the distance to the wall, κ and B are model parameters, and the $+$ superscript refers to the value being expressed in wall units: $u^+ = \langle u\rangle/\langle u_\tau\rangle$ and $y^+ = y\langle u_\tau\rangle/\nu$, where $\langle u_\tau\rangle = \sqrt{\langle\tau_w\rangle/\rho}$ is the mean friction velocity.

Given $\langle u\rangle$ at a point y, the above law provides an equation to calculate $\langle u_\tau\rangle$ and thus $\langle\tau_w\rangle$. An important feature of the Spalding law of the wall is that it is differentiable with respect to $\langle u_\tau\rangle$. This allows employing the Newton-Raphson method to solve (9).

While (9) is written for averaged quantities the idea is to solve this equation at every time-step to get an approximation of the *instantaneous* value of the friction velocity and thus of the instantaneous wall shear stress. The discussion of the relationship between the quantities appearing in (9) and the LES simulation is continued in the next section.

Before proceeding, a comment is given regarding the model coefficients employed in [26]. While the values of κ and B were originally suggested to be 0.4 and 5.5 [26], respectively, different flow-dependent values have been found for them due to more recent experimental data. For instance, Nagib and Chauhan [17] showed that at sufficiently high Reynolds numbers the Kármán coefficient κ for channel flow is approximately 0.37 which is smaller than the value of 0.384 found for zero-pressure-gradient (ZPG) boundary layers (e.g. see [19]), which is in turn less than what is calculated for pipe flow. Accordingly, the coefficient B was estimated to be 3.7, 4.17, and 5.0 for channel, ZPG-TBL, and pipe flows, respectively, [17]. It must be emphasized that there are no universal values for the above-mentioned parameters, and depending on the estimation method and assumption on the limits of different regions within the boundary layer, they will vary, e.g. see [18].

3.2.3 The input to the model

To completely define the model, the relationship between $\langle u \rangle$, y, and the quantities used in the LES simulation has to be considered. That is, Step 1 of the algorithm outlined in Section 3.2.1.

In equation (9), y is the distance from the wall. This quantity has to be related to the distance from the face centre f to some point in the domain of the LES simulation. One natural choice is a point located at some specified distance away from f along the face-normal direction. Another alternative, attractive due to its simplicity and employed here, is to consider P, that is, the cell centre of the cell that the considered face belongs to. In that case y is the distance between f and P. The advantage of this choice is that all the quantities from the LES simulation are readily available at P, therefore no interpolation has to be performed. However, on an arbitrary (non-orthogonal) mesh the distance from f to P is not equal to the distance between P and the wall, which introduces an error.

The quantity $\langle u \rangle$ in (9) is the mean value of the wall-parallel component of velocity. From the LES simulation, on the other hand, the Cartesian components of the instantaneous filtered velocity values, $\overline{v}_i$, are available. Different ways of relating $\langle u \rangle$ and $\overline{v}_i$ can be thought of.

One consideration is whether to actually use the instantaneous quantities or to instead perform averaging of $\overline{v}_i$ in the course of the simulation (say, over some reasonable time window T) and use the result of that. The latter approach was used in the earlier works [25, 10], where the temporally and spatially averaged velocity was used as input to the wall function. However, the instantaneous local velocity has also been used, see e.g. [16]. In [2, 3], Cabot et al reported that no significant difference between the results achieved by employing these two paradigms was found. Therefore, for the sake of simplicity, here the instantaneous filtered quantities, $\overline{v}_i$ are used.

Another aspect is whether to consider the magnitude of the filtered velocity vector or of its wall-parallel projection. Here, the former is used. The rationale is that even for the instantaneous quantity the size of the wall-normal component is negligibly small, as compared to the wall-parallel one. However, to the best of the authors' knowledge no study on the effect of this approximation has been reported.

To summarize, $\langle u \rangle$ in (9) is substituted with the magnitude of the instantaneous filtered velocity taken at the cell centre P of the cell which the considered wall-face belongs to. The distance from P to the wall (y in (9)) is approximated by the distance between P and the centre of the face f. Provided this input, equation (9) is solved in order to provide the value of the instantaneous friction velocity that, in turn, allows to compute the wall shear stress $\overline{\tau}_w$.

3.2.4 Enforcing the wall shear stress

All the components for using the wall model to compute the wall shear stress are now in place. What remains to be discussed is how the obtained value $\overline{\tau}_w$ is fed back into the discrete formulation of the large-eddy simulation.

The key relation is equation (8) for the wall shear stress at a cell face. Considering a subgrid stress model in the bulk of the domain which contains a subgrid viscosity, $\tau_{ij}^{\mathrm{sgs}} = 2\nu_{\mathrm{sgs}}\overline{s}_{ij}$. The standard finite-volume approximation of the diffusive term, together with no-slip conditions on $\overline{v}_i$, then gives the following relations.

$$\overline{\tau}_{w,12} = (\nu + \nu_{\mathrm{sgs}})_f \frac{\overline{v}_{1,P}}{\Delta x_2}, \qquad \overline{\tau}_{w,32} = (\nu + \nu_{\mathrm{sgs}})_f \frac{\overline{v}_{3,P}}{\Delta x_2} \tag{10}$$

The sub-script P implies evaluation in the cell center and the sub-script f evaluation in the face center. In case a subgrid viscosity is not employed in the bulk of the domain, a separate field can be introduced for the needs of the wall model. The correct value of the wall shear stress, $\overline{\tau}_w$, is then enforced if the following value of ν_{sgs} is set on the cell face (in each time step).

$$\nu_{\mathrm{sgs}} = \frac{\overline{\tau}_w}{\left[\left(\overline{v}_{1,P}/\Delta x_2\right)^2 + \left(\overline{v}_{3,P}/\Delta x_2\right)^2\right]^{1/2}} - \nu \tag{11}$$

In summary, the wall shear stress is computed from the cell-center velocity using Spalding's law, then the subgrid viscosity is modified on the wall boundary which in turn affects the momentum equation through the boundary condition and the discretization of the diffusion term. It is necessary in this process to employ the no-slip boundary condition for $\overline{v}_i$ at the wall.

4 Application to channel flow

The aim of this section is to illustrate how the wall-modelled LES machinery explained in detail in the previous sections can be applied to a canonical wall-bounded turbulent flow and what level of accuracy can be expected from such a computation. For this

purpose, turbulent channel flow was simulated using the the finite-volume based solver `OpenFOAM`.

A computational domain of size $L_x \times L_y \times L_z = 9\delta \times 2\delta \times 4\delta$ was used. The channel half-height δ and the bulk velocity $\bar{U}$ were taken to be 1 m and 1 m/s, respectively. The flow was computed for several values of the bulk Re-number, $\mathrm{Re} = \bar{U}\delta/\nu$, corresponding to those found in the DNS of Lee and Moser [14], which is used as reference. The change in Re was achieved through modifying the value of the kinematic viscosity, ν, as represented in Table 1.

Table 1: Different Re-numbers for which DNS-data [14] exists. Both $\mathrm{Re} = \bar{U}\delta/\nu$ and $\mathrm{Re}_\tau = u_\tau\delta/\nu$ are achieved by adjusting ν, keeping the rest of the parameters fixed. The value of Re given in the table is an input parameter, while the value of Re_τ is computed by DNS.

Re	Re_τ	$\nu(\mathrm{m}^2/\mathrm{s})$
10 000	543.4	10^{-4}
20 000	1 000.5	$5 \cdot 10^{-5}$
43 478	1 994.8	$2.3 \cdot 10^{-5}$
125 000	5 185.9	$8 \cdot 10^{-6}$

For all simulated cases, the domain was discretised with $270 \times 60 \times 120$ cubical hexahedral cells, that is, with 1 944 000 cells in total and 27 000 cells in a δ^3-cube. This number is somewhat higher than what was used in previous similar studies. According to the guideline proposed by Chapman [5], 2 500 cells per δ^3 would be adequate for WMLES of a turbulent boundary layer with thickness δ. For channel flow, examples of previously employed resolutions are 1 000 [21], 1 250 [4], and 4 100 [25] points per δ^3. However, what is important is that the mesh size employed here is still negligibly small compared to what a WRLES would require.

Time step $\Delta t = 0.01$ s was chosen in all simulations and flow statistics were computed over 300 s after initial transients were removed. The simulations were run in parallel on 48 processors for over 28 hours of wall clock time including both the transient removal and statistical averaging phases.

The face-centre values, needed for the discretisation of the governing equations (see Section 2.2), were computed using linear interpolation between the values at the centres of the cells sharing the face, which, along with a central-difference scheme for the viscous terms, results in a spatially second-order accurate method. In time, a second order implicit backward-differencing scheme was used, see [11] for details. For SGS modelling in the interior of the domain, the dynamic one-equation model of Kim and Menon [12] was employed, with the associated length scale taken to be equal to the cubic root of the local cell volume.

The values of Re_τ computed by WMLES are compared to the DNS values of [14] in Table 2. A systematic under-prediction is observed. It is worth mentioning that the

Table 2: Computed values of Re_τ and the associated relative error as compared to the DNS data.

DNS	WMLES	Relative Error (%)
553	527	4.70
1 001	933	6.79
1 995	1 842	7.67
5 186	4 803	7.39

relative error in Re_τ increases slightly from $Re = 10\,000$ to $20\,000$, but it remains almost unchanged from there to the two highest Re-numbers. This shows the robustness of the employed methodology.

Mean velocity profiles at different Re-numbers computed by WMLES are compared to the DNS data in Figure 2. In all cases, the WMLES mean velocity values in inner scaling are over-predicted while there is a good agreement between the velocities in outer scaling. This is a reflection of the fact that magnitude of u_τ in WMLES is under-predicted, which has already been observed above through the under-prediction of Re_τ (see Table 2).

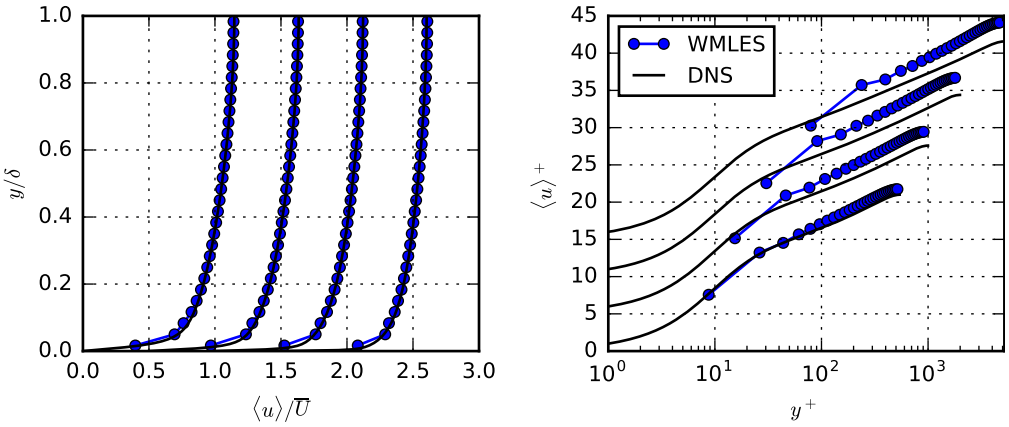

Figure 2: Mean velocity profiles in outer scaling (left) and inner scaling (right). Comparison between DNS and WMLES for the four computed Re-numbers. For increasing Re, the profiles in outer scaling are shifted by $0.5\bar{U}$, and in inner scaling profiles by $5u_\tau$.

There are different factors that affect the results of WMLES including the accuracy of the numerical scheme that is second-order here, cell density, the performance of the SGS model and the choice of wall model. It is not straightforward to figure out which of these factors or a specific combination of them may be the main responsible for the under-prediction of the shear stress in the present study. For example, it can be expected that the SGS model, when acting on a coarse grid near the wall, is not capable of calculating the subgrid stresses correctly, even through a dynamic procedure [4, 20]. It is therefore important to reiterate that the purpose of the current study is merely to

illustrate what general level of accuracy one can expect from a WMLES employing a simple wall-stress model. It also demonstrates the enormous savings in computational resources this approach has to offer. For $\mathrm{Re}_\tau \approx 5200$ the DNS results where obtained using 120.8 *billion* computational nodes [14], whereas 1.94 million cells where used in the WMLES.

5 Concluding remarks

This report provides the formulation and a detailed description of a wall-stress model based on the Spalding law of the wall, implemented within the framework of a collocated finite-volume solver. Its applicability to simulation of canonical turbulent flows is illustrated by a series of channel flow simulations covering a range of Reynolds numbers.

Due to the fact that Spalding's law of the wall [26] is valid throughout the whole inner and log-law layer, the model is extremely robust. Also, the applicability of the Newton-Raphson method to solving the non-linear equation (9) that constitutes the model makes it efficient.

Several components of the model could potentially be improved. This includes choosing more optimal values of κ and B, considering the wall-parallel projection of the velocity vector instead of its total magnitude, and computing the distance from the cell centre to the boundary in a more accurate manner. To what extent these changes can improve the performance of the model is subject to further research. However, the results shown in Section 4 indicate that even without modification the considered wall model can be successfully utilised.

References

[1] S. T. Bose and P. Moin. A dynamic slip boundary condition for wall-modeled large-eddy simulation. *Physics of Fluids*, 26:015104, 2014.

[2] W. Cabot. Large-eddy simulations with wall models. *Center for Turbulence Research, Annual Research Brief*, pages 41–50, 1995.

[3] W. Cabot, J. Jiménez, and J. S. Baggett. On wakes and near-wall behavior in coarse large-eddy simulation of channel flow with wall models and second-order finite-difference methods. *Center for Turbulence Research, Annual Research Brief*, pages 343–354, 1999.

[4] W. Cabot and P. Moin. Approximate wall boundary conditions in the large-eddy simulation of high Reynolds number flow. *Flow, Turbulence and Combustion*, 63(1):269–291, 2000.

[5] D. R. Chapman. Computational aerodynamics development and outlook. *AIAA Journal*, 17(12):1293–1313, 1979.

[6] H. Choi and P. Moin. Grid-point requirements for large eddy simulation: Chapmans estimates revisited. *Physics of Fluids*, 24:011702, 2012.

[7] E. de Villiers. *The potential of large-eddy simulation for the modeling of wall-bounded flows*. PhD thesis, Imperial College London, 2006.

[8] J. Ferziger and M. Peric. *Computational Methods for Fluid Dynamics*. Springer, 2001.

[9] C. Fureby. On LES and DES of Wall Bounded Flows. ERCOFTAC Bulletin, March 2007.

[10] G. Grötzbach. *Direct numerical and large eddy simulations of turbulent channel flows*, volume 6 of *Encyclopedia of Fluid Mechanics, Complex Flow Phenomena and Modeling*, pages 1337–1391. Gulf Publishing, 1987.

[11] H. Jasak. *Error analysis and estimation for the finite volume method with applications to fluid flows*. PhD thesis, Imperial College of Science, Technology and Medicine, 1996.

[12] W. Kim and S. Menon. A new dynamic one-equation subgrid-scale model for large eddy simulation. Reno, NV, 1995. 33rd Aerospace Sciences Meeting and Exhibit.

[13] J. Larsson, S. Kawai, J. Bodart, and I. Bermejo-Moreno. Large-eddy simulation with modeled wall-stress: recent progress and future directions. *Bulletin of the JSME*, 3(1):1–23, 2016.

[14] M. Lee and R. D. Moser. Direct numerical simulation of turbulent channel flow up to $\mathrm{Re}_\tau \approx 5200$. *Journal of Fluid Mechanics*, 774:395–415, 2015.

[15] T. Marić, J. Höpken, and K. Mooney. *The OpenFOAM Technology Primer.* sourceflux, 2014.

[16] P. J. Mason and N. S. Callen. On the magnitude of the subgrid-scale eddy coefficient in large-eddy simulations of turbulent channel flow. *Journal of Fluid Mechanics*, 162:439–462, 1986.

[17] H. M. Nagib and K. A. Chauhan. Variations of von Kármán coefficient flows. *Physics of Fluids*, 20:101518, 2008.

[18] R. Örlü, J. H. M. Fransson, and P. H. Alfredsson. On near wall measurements of wall bounded flows-the necessity of an accurate determination of the wall position. *Progress in Aerospace Sciences*, 46:353–387, 2010.

[19] J. M. Österlund, A. Johansson, H. M. Nagib, and M. H. Hites. A note on the overlap region in turbulent boundary layers. *Physics of Fluids*, 12(1):1–4, 2000.

[20] U. Piomelli and E. Balaras. Wall-layer models for large-eddy simulations. *Annu. Rev. Fluid Mech.*, 34:349–374, 2002.

[21] U. Piomelli, J. Ferziger, P. Moin, and J. Kim. New approximate boundary conditions for large eddy simulations of wall-bounded flows. *Physics of Fluids A*, 1(6):1061–1068, 1989.

[22] S. Rezaeiravesh, M. Liefvendahl, and C. Fureby. On grid resolution requirements for LES of wall-bounded flows. In *VII European Congress on Computational Methods in Applied Sciences and Engineering*, Crete, Greece, June 2016.

[23] P. Sagaut. *Large eddy simulation for incompressible flows.* Springer-Verlag, 2nd edition, 2002.

[24] H. Schlichting. *Boundary-layer theory.* McGraw-Hill, 7th edition, 1979.

[25] U. Schumann. Subgrid scale model for finite difference simulations of turbulent flows in plane channels and annuli. *Journal of Computational Physics*, 18(4):376–404, 1975.

[26] D. B. Spalding. A Single Formula for the "Law of the Wall". *Journal of Applied Mechanics*, pages 455–458, 1961.

[27] H. G. Weller, G. Tabor, H. Jasak, and C. Fureby. A tensorial approach to computational continuum mechanics using object-oriented techniques. *Computers in Physics*, 12(9):620–631, 1998.

Recent technical reports from the Department of Information Technology

2016-017 S.-E. Ekström and S. Serra-Capizzano: *Eigenvalues of Banded Symmetric Toeplitz Matrices are Known Almost in Close Form?*

2016-016 Torsten Söderström and Umberto Soverini: *Errors-in-Variables Identification using Maximum Likelihood Estimation in the Frequency Domain*

2016-015 Afshin Zafari, Elisabeth Larsson, Marco Righero, M. Alessandro Francavilla, Giorgio Giordanengo, Francesca Vipiana, and Giuseppe Vecchi: *Task Parallel Implementation of a Solver for Electromagnetic Scattering Problems*

2016-014 Vasilis Spiliopoulos, Andreas Sembrant, Georgios Keramidas, Erik Hagersten, and Stefanos Kaxiras: *A Unified DVFS-Cache Resizing Framework*

2016-013 Elias Castegren and Tobias Wrigstad: *LOLCAT: Relaxed Linear References for Lock-free Programming*

2016-012 Marco Donatelli, Paola Novara, Lucia Romani, Stefano Serra-Capizzano, and Debora Sesana: *Surface Subdivision Algorithms and Structured Linear Algebra: a Computational Approach to Determine Bounds of Extraordinary Rule Weights*

2016-011 Ken Mattsson: *Diagonal-Norm Upwind SBP Operators*

2016-010 Afshin Zafari, Elisabeth Larsson, and Martin Tillenius: *DuctTeip: A Task-Based Parallel Programming Framework for Distributed Memory Architectures*

2016-009 Andreas Svensson: *On the Role of Monte Carlo Methods in Swedish M. Sc. Engineering Education*

2016-008 Andreas Svensson and Thomas B. Schön: *Comparing Two Recent Particle Filter Implementations of Bayesian System Identification*

2016-007 Elias Castegren and Tobias Wrigstad: *Reference Capabilities for Trait Based Reuse and Concurrency Control*

2016-006 Josefin Ahlkrona: *The ISCAL method and the Grounding Line - Combining the Stokes equations with the Shallow Ice Approximation and Shelfy Stream Approximation*

UPPSALA
UNIVERSITET

January 2017
ISSN 1404-3203
http://www.it.uu.se/